Research Article

OPEN ACCESS

SCC Publishing
Michelets vei 8 B
1366 Lysaker Norway

ISSN: 2703-9072

Correspondence:
cohler@post.harvard.edu

Vol. 6.4 (2026)
pp. 81–99

Mathematical Falsification of the Fossil-Dominant Hypothesis for Rising Atmospheric CO_2 Using the Keeling Relation

Jonathan Cohler[1]*, *Willie Soon*[2]

[1]*Cohler & Associates, Inc., Lexington, MA 02420, USA* • cohler@post.harvard.edu
[2]*Institute of Earth Physics and Space Science, 9400 Sopron, Hungary* • soon.willie@epss.hu

Abstract

The IPCC, NASA, NOAA, and EPA state that essentially all of the observed rise in atmospheric CO_2 since the pre-industrial era originates from fossil-fuel combustion. This paper shows that claim is mathematically inconsistent with the isotopic record those same agencies rely on. The Keeling plot of $\delta^{13}C$ against $1/C$ has an intercept $\delta^{13}C_I$ equal to the flux-weighted isotopic signature of the net carbon addition to the atmosphere. Applied by Koutsoyiannis (2024a) [16] to instrumental $\delta^{13}C$ records from four Scripps CO_2 Program stations (Barrow, La Jolla, Mauna Loa, South Pole) spanning about 1978 to present, this construction gives $\delta^{13}C_I = -13.2 \pm 0.2$‰. Caribbean sclerosponge $\delta^{13}C$ reconstructions of surface-water dissolved inorganic carbon by Böhm et al. (2002) [2] extend this value back to approximately 1500 AD with no significant drift. Independent Keeling regression of the Law Dome ice-core record by Kohler et al. (2006) [14] yields the same intercept with $r^2 = 0.96$. The two-endmember mixture equation $\delta^{13}C_I = f\,\delta^{13}C_F + (1-f)\,\delta^{13}C_N$, using the standard fossil signature $\delta^{13}C_F \approx -28$‰ and the physically admissible range -13.2‰ $\leq \delta^{13}C_N \leq -8$‰, forces the fossil fraction f of the net addition into the interval $[0, 0.26]$. Even under the counterfactual relaxation $\delta^{13}C_N = 0$‰, well outside any physically realizable natural-reservoir signature, f is bounded above by 0.471. The five-century invariance of $\delta^{13}C_I$ across a roughly 10^4-fold increase in fossil emissions further collapses the admissible band to $f \approx 0$. The claim of fossil dominance is therefore not merely empirically weak; it is inconsistent with the arithmetic of the isotopic constraint applied to the standard measurement record. The rejection of the conclusion requires the rejection of one of three inputs: elementary mass-balance algebra, the standard isotopic endmember values used throughout the carbon-cycle literature, or the primary Scripps and sclerosponge datasets themselves.

Keywords: atmospheric CO_2; carbon isotopes; Keeling plot; fossil-fuel attribution; carbon cycle; $\delta^{13}C$; sclerosponge proxy; mass balance; IPCC

Submitted 2026-08-25, Accepted 2026-10-21. https://doi.org/10.53234/scc202612/05

1. Introduction

The attribution of essentially all post-industrial CO_2 rise to fossil-fuel combustion is the foundational premise of contemporary carbon-cycle assessment. It appears in IPCC AR6 Chapter 5 by Canadell et al. (2021) [3], in the annual Global Carbon Budget of Friedlingstein et al. (2026) [7], and in the public communications of NASA, NOAA, EPA, and the World Meteorological Organization. The premise flows directly into projections of concentration pathways, into calculations of Global Warming Potential based on the Bern impulse response function, and into national and

international emissions accounting.

The premise is testable. Fossil carbon carries a distinct isotopic fingerprint, near −28‰ on the VPDB scale, as compiled by Andres et al. (2000) [1]. This signature is inherited from C3 photosynthesis of the source biomass hundreds of millions of years ago, discussed by Kohn (2010) [15]. Natural carbon reservoirs relevant to atmospheric exchange carry heavier signatures. Ocean dissolved inorganic carbon sits near +1.5‰, releasing CO_2 at approximately −8‰ after gas-DIC fractionation of about 9‰ at surface ocean temperatures, as measured by Mook (1986) [20] and Zhang et al. (1995) [27]. Volcanic and mantle carbon sits around −5‰, as reviewed by Deines (2002) [5]; carbonate weathering carbon sits near 0‰. Terrestrial respiration returns carbon at approximately −25‰ [15], reflecting the source biomass of the growing season.

If the net addition to the atmosphere were dominated by any single reservoir, the flux-weighted mean isotopic signature of that net addition would be constrained to sit near the signature of the dominant source. This is not a subtle inference. It is elementary two-endmember mixing.

The Keeling plot, introduced by Keeling (1958) [11] and used as a standard diagnostic across the carbon-cycle literature for more than six decades, provides direct access to the flux-weighted mean signature of the net addition. The plot of δ^{13}C against $1/C$ has an intercept equal to $\delta^{13}C_I \equiv F_{13}/F_{12}$ converted to delta notation, where F_{12} and F_{13} are the net fluxes of the light and heavy isotopes into the reservoir. The construction is derived from conservation of mass alone. It requires no assumptions about individual source or sink processes, no modeling of ocean chemistry, no biosphere parameterization, and no atmospheric transport scheme.

The Keeling construction applied to instrumental δ^{13}C records from four Scripps CO_2 Program monitoring sites spanning approximately 1978 to present obtains $\delta^{13}C_I = -13.2 \pm 0.2$‰ [16]. Surface-water dissolved inorganic carbon δ^{13}C reconstructed from the Caribbean sclerosponge *Ceratoporella nicholsoni* back to approximately 1500 AD yields a value that hovers near −13‰ across the full five-century record [2]. The intercept is stable across a period during which global fossil emissions rose from essentially zero to approximately 10 GtC/yr.

The observation is the answer to the mixing question. The purpose of this paper is to make the deduction explicit and to identify which of the standard inputs a rejection of the deduction would require rejecting.

Section 2 sets out the notation. Section 3 derives the Keeling intercept relation from mass conservation. Section 4 states the observations. Section 5 performs the mixture decomposition and establishes the admissible range of the fossil fraction. Section 6 tests robustness by relaxing the natural-signature upper bound beyond physical plausibility. Section 7 uses the five-century constancy of the intercept to collapse the admissible band to a single point. Section 8 identifies the three input categories a rejection of the conclusion would require rejecting. Section 9 discusses relation to the existing carbon-cycle literature and the scope of the claim. Section 10 concludes.

2. Notation and Definitions

$C \equiv$ total carbon mass in the atmospheric reservoir
C_{12}, $C_{13} \equiv$ masses of the two stable isotopes, $C = C_{12} + C_{13}$
$R \equiv C_{13}/C_{12}$, the isotopic ratio of the reservoir
$R_{\text{std}} \equiv 0.0111802$, the VPDB reference ratio compiled by Werner and Brand (2001) [26]
$\delta^{13}\text{C} \equiv 1000\,(R/R_{\text{std}} - 1)$, the reservoir signature in per-mil notation
$F_{12} \equiv dC_{12}/dt$, net atmospheric flux of the light isotope
$F_{13} \equiv dC_{13}/dt$, net atmospheric flux of the heavy isotope
$F_{\text{net}} \equiv dC/dt = F_{12} + F_{13}$, net total-carbon flux
$R_I \equiv F_{13}/F_{12}$, isotopic ratio of the net incoming flux

$\delta^{13}C_I \equiv 1000\,(R_I/R_{\text{std}} - 1)$, signature of the net incoming flux
$\delta^{13}C_F \equiv -28‰$, standard fossil signature [1]
$\delta^{13}C_N \equiv$ flux-weighted mean signature of the natural (i.e. non fossil fuel) residual net flux
$f \equiv$ fossil fraction of F_{net} $(0 \le f \le 1)$

Small-ratio approximation. The natural abundance of ^{13}C is about 1.1%, so $R,\ R_I \approx 0.011 \ll 1$. To leading order $C_{12} \approx C$ and $F_{13} \approx F_{\text{net}} R_I$.

Note: the exact derivation retaining factors of $1 + R$ *shifts the extracted intercept by under* $0.01‰$*, well below the measurement precision of the underlying* $\delta^{13}C$ *record.*

3. Derivation of the Keeling Intercept Relation

3.1 Conservation of each isotope

Total atmospheric carbon and each individual isotope are separately conserved:

$$\frac{dC}{dt} = F_{\text{net}}, \qquad \frac{dC_{13}}{dt} = F_{13} \approx F_{\text{net}}\, R_I. \tag{1}$$

The second relation uses the small-ratio approximation above.

3.2 Isotope balance in delta form

From the definition of $\delta^{13}C$ we have $C\,\delta^{13}C = 1000\,(C_{13}/R_{\text{std}} - C)$. Differentiating with respect to time and substituting Eq. (1):

$$\begin{aligned} \frac{d(C\,\delta^{13}C)}{dt} &= \frac{1000}{R_{\text{std}}}\,\frac{dC_{13}}{dt} - 1000\,\frac{dC}{dt} \\ &\approx \frac{1000}{R_{\text{std}}}\,F_{\text{net}}\,R_I - 1000\,F_{\text{net}} \\ &= F_{\text{net}}\,\delta^{13}C_I. \end{aligned} \tag{2}$$

3.3 The Keeling relation

Expanding the left side of Eq. (2) and substituting $dC/dt = F_{\text{net}}$:

$$C\,\frac{d(\delta^{13}C)}{dt} + \delta^{13}C \cdot F_{\text{net}} = F_{\text{net}}\,\delta^{13}C_I \quad\Longrightarrow\quad \frac{d(\delta^{13}C)}{\delta^{13}C_I - \delta^{13}C} = \frac{dC}{C}. \tag{3}$$

Integrating from an initial state $(C_0, \delta^{13}C_0)$:

$$\delta^{13}C(C) = \delta^{13}C_I + (\delta^{13}C_0 - \delta^{13}C_I)\,\frac{C_0}{C}. \tag{4}$$

A plot of $\delta^{13}C$ against $1/C$ is therefore a straight line with intercept $\delta^{13}C_I$, so a linear regression on the record extracts the flux-weighted signature of the net atmospheric addition directly.

Note: Eq. (4) is the Keeling plot relation [11], used as a standard diagnostic throughout the carbon-cycle literature for over six decades. It is not new. What follows are its necessary logical consequences when combined with the observed value of $\delta^{13}C_I$ *and the standard endmember signatures.*

The intercept $\delta^{13}C_I$ is the flux-weighted mean signature of the net addition, integrated across all sources and sinks that contribute to F_{net}. It is not a source-only quantity, and it is not a modeled quantity. It is directly readable from a linear regression of $\delta^{13}C$ on $1/C$ in any atmospheric $\delta^{13}C$ record for which the small-ratio approximation holds.

4. The Observed Intercept

4.1 Four-site instrumental record

The Keeling regression has been performed on instrumental δ^{13}C records from four independent monitoring sites in the Scripps CO_2 Program network [16]:

- Point Barrow, Alaska, approximately 71°N;
- La Jolla Pier, California, approximately 33°N;
- Mauna Loa Observatory, Hawaii, approximately 20°N;
- South Pole, Antarctica, approximately 90°S.

The four sites span the full latitudinal range of the marine boundary layer, from Arctic to Antarctic, with instrumental δ^{13}C records that began at various dates from about 1978 onward. Each individual site yields an intercept consistent with

$$\delta^{13}\mathrm{C}_I = -13.2 \pm 0.2‰, \tag{5}$$

with the four-site pooled analysis returning the same value (see Figure 10 of Koutsoyiannis (2024a) [16]).

The Scripps CO_2 Program is the primary source of long-term high-precision atmospheric δ^{13}C measurements. Its records are used as the isotopic input in IPCC assessment cycles. The measurement precision on individual δ^{13}C values is typically better than 0.05‰; the ±0.2‰ uncertainty on the intercept reflects site-to-site variation and residual regression scatter, not instrumental uncertainty.

4.2 Five-century proxy extension

The δ^{13}C of surface-water dissolved inorganic carbon has been reconstructed from a Caribbean sclerosponge (*Ceratoporella nicholsoni*) with sub-annual growth banding, extending back to approximately 1500 AD [2]. Sclerosponge skeletal aragonite records DIC δ^{13}C with a small and stable fractionation offset. The reconstructed surface-water DIC δ^{13}C translates to an atmospheric $\delta^{13}\mathrm{C}_I$ that hovers near

$$\delta^{13}\mathrm{C}_I \approx -13‰ \tag{6}$$

across the full five-century record, with no significant drift.

The proxy extension measurement is totally independent of the instrumental Scripps record. Its agreement with Eq. (5) is therefore an independent confirmation of the intercept value, obtained from a different medium, a different signal transfer function, and a different laboratory pipeline.

4.3 Law Dome ice-core confirmation

An independent third confirmation of the intercept value is obtained from Antarctic ice-core CO_2 and δ^{13}C data. Kohler et al. (2006) [14] analyzed the Law Dome ice-core record and reported a Keeling regression of δ^{13}C against $1/C$ that yields an intercept of approximately −13‰ with $r^2 = 0.96$. The high r^2 confirms that the Keeling relation Eq. (4), a direct consequence of mass conservation, holds across the ice-core record just as it holds across the instrumental Scripps record of §4.1 and the sclerosponge reconstruction of §4.2.

The Law Dome record shares no measurement chain with either the Scripps instrumental record or the Caribbean sclerosponge reconstruction. Its intercept agreement therefore constitutes a third independent confirmation of $\delta^{13}\mathrm{C}_I \approx -13‰$, obtained from a different medium (ice-core enclosed air), a different signal-transfer function (firn-air diffusion and bubble enclosure), a different geographic location (East Antarctica), and a different laboratory pipeline. The three-way convergence of instrumental, sclerosponge, and ice-core intercepts across five centuries and across essentially

independent measurement systems removes any residual concern that the value is a measurement or reconstruction artifact.

Kohler et al. (2006) [14] is among the datasets cited in the carbon-cycle literature in support of anthropogenic attribution of the CO_2 rise. Its own Keeling regression, however, is fully consistent with the intercept obtained from the Scripps instrumental record and from the sclerosponge proxy, and forces the same conclusion Eq. (13) through the mixture equation Eq. (8).

5. Falsification of Fossil Dominance

5.1 Two-endmember decomposition

The flux-weighted mean signature of the net addition, weighting the fossil endmember by its share f (defined in §2) and the natural residual by $1 - f$ (both of which positive fractions between 0 and 1), is

$$\delta^{13}\mathrm{C}_I = f\,\delta^{13}\mathrm{C}_F + (1 - f)\,\delta^{13}\mathrm{C}_N, \tag{7}$$

with $\delta^{13}\mathrm{C}_F \approx -28‰$ [1] and $\delta^{13}\mathrm{C}_N$ the flux-weighted mean signature of the natural, i.e. non-anthropogenic, residual net flux. Solving for f:

$$f = \frac{\delta^{13}\mathrm{C}_I - \delta^{13}\mathrm{C}_N}{\delta^{13}\mathrm{C}_F - \delta^{13}\mathrm{C}_N} = \frac{-13.2 - \delta^{13}\mathrm{C}_N}{-28 - \delta^{13}\mathrm{C}_N} = \frac{13.2 + \delta^{13}\mathrm{C}_N}{28 + \delta^{13}\mathrm{C}_N}. \tag{8}$$

5.2 Physical bounds on the natural signature

Upper bound: $\delta^{13}\mathrm{C}_N \le -8‰$. Ocean-atmosphere gas exchange is the dominant natural component of the atmospheric CO_2 flux over multi-annual timescales. Surface-ocean DIC sits near +1.5‰, as measured by Kroopnick (1985) [18] and Quay et al. (1992) [21]; the gas-DIC equilibrium fractionation at surface ocean temperatures is approximately −9‰ [20, 27]. Ocean-outgassed CO_2 therefore carries a signature near −8‰. Volcanic emissions carry a signature of approximately −5‰ [5][1] and carbonate weathering carries a signature near 0‰; both are quantitatively smaller components with heavier signatures, so they do not shift the flux-weighted natural mean signature significantly lighter than the ocean value (Figure 1).

Lower bound: $\delta^{13}\mathrm{C}_N \ge -13.2‰$. The requirement $f \ge 0$ (fossil emissions cannot subtract carbon from the atmosphere) forces the numerator $13.2 + \delta^{13}\mathrm{C}_N$ in Eq. (8) to be non-negative. This gives $\delta^{13}\mathrm{C}_N \ge -13.2‰$ as a hard floor (Figure 1).

5.3 The fossil fraction across the admissible range

Evaluating Eq. (8) across the admissible interval $-13.2‰ \le \delta^{13}\mathrm{C}_N \le -8‰$ using the modern instrumental intercept $\delta^{13}\mathrm{C}_I = -13.2 \pm 0.2‰$ from the 44-year Scripps four-site record:

- At the lower bound $\delta^{13}\mathrm{C}_N = -13.2‰$: $f = 0$.
- At the upper bound $\delta^{13}\mathrm{C}_N = -8‰$: $f = (13.2 - 8)/(28 - 8) = 5.2/20 = 0.26$.

Across the full admissible range, the instrumental record alone bounds the fossil fraction at

$$f \in [0,\ 0.26] \qquad \text{(instrumental window; Figure 1).} \tag{9}$$

No value of $\delta^{13}\mathrm{C}_N$ within the physically admissible range permits fossil dominance ($f > 0.5$; Figure 1). The maximum admissible fossil fraction of the net atmospheric CO_2 addition over the 44-year instrumental window is 26%. This bound is tightened to $f \approx 0$ by the five-century sclerosponge constancy result of §7.

[1] "A major fraction of the Earth's deep carbon reservoir has δ^{13}C values around −5‰, as manifested by volcanic CO_2 exhalations . . ." Deines (2002) [5].

6. Robustness Under Counterfactual Relaxation

The upper bound $\delta^{13}C_N \leq -8‰$ derived above rests on the standard oceanographic values for surface DIC composition and gas-DIC fractionation. Both are direct measurement results from the carbon-isotope literature and are used without dispute in IPCC assessments. Nevertheless, this section tests robustness by removing the upper bound entirely and asking how much lighter the required natural signature would have to become for the conclusion to reverse.

Setting $\delta^{13}C_N = 0‰$ (the VPDB standard itself, heavier than any natural carbon reservoir on Earth's surface), Eq. (8) gives

$$f = \frac{13.2 + 0}{28 + 0} = \frac{13.2}{28} = 0.471 = 47.1\%, \tag{10}$$

still below a majority (Figure 1). Fossil dominance $f > 0.5$ would require $\delta^{13}C_N > +1.6‰$ (Figure 1), a value not approached by any known terrestrial or oceanic reservoir. The claim of fossil dominance of the net atmospheric CO_2 addition is therefore falsified across every physically conceivable value of $\delta^{13}C_N$, not merely across the physically realistic range.

The IPCC-consistent position $f \approx 1$ is reached only as $\delta^{13}C_N \to +\infty$, which is not physically possible (Figure 1).

7. The Constancy Constraint

The mixture equation Eq. (8) applies at every moment for which the Keeling regression can be performed. Global fossil CO_2 emissions rose from approximately 2.5 GtC/yr at the start of the Mauna Loa CO_2 record in 1959 to approximately 10 GtC/yr in 2023 [7], a factor of about four. Across the sclerosponge proxy extension back to about 1500 AD, fossil emissions grew from essentially zero to the same present value, spanning roughly four orders of magnitude in fossil source strength.

If f were significant, the intercept $\delta^{13}C_I$ would drift toward $\delta^{13}C_F \approx -28‰$ as the fossil-emission strength grew, because the fossil signature would pull the flux-weighted mean net-addition signature toward the fossil value in proportion to the fossil share of F_{net}. The intercept did not drift. Across the full five-century sclerosponge record, $\delta^{13}C_I$ shows no significant secular drift, and its long-term mean is consistent with the modern instrumental value $\delta^{13}C_I = -13.2 \pm 0.2‰$ from the Scripps four-site record and the Law Dome ice-core intercept of Kohler et al. (2006) [14].

Applying the mixing equation at the two endpoints of the record makes the collapse to $f \approx 0$ quantitative. At the pre-industrial reference date ($t_0 \approx 1500$ AD), fossil emissions were negligible, so $f(t_0) \approx 0$, and Eq. (7) reduces to $\delta^{13}C_I(t_0) = \delta^{13}C_N(t_0)$. The sclerosponge reconstruction gives $\delta^{13}C_I(t_0) \approx -13‰$, which fixes the natural signature at

$$\delta^{13}C_N(t_0) \approx -13‰. \tag{11}$$

The natural signature $\delta^{13}C_N$ is set by the ocean-atmosphere carbon cycle, buffered on multi-century timescales by the large ocean DIC reservoir; the observed constancy of $\delta^{13}C_I$ across the record implies $\delta^{13}C_N(t) \approx -13‰$ throughout. Solving Eq. (8) for the modern value with $\delta^{13}C_I = -13.2‰$ and $\delta^{13}C_N \approx -13‰$:

$$f_{\text{modern}} = \frac{\delta^{13}C_I - \delta^{13}C_N}{\delta^{13}C_F - \delta^{13}C_N} = \frac{-13.2 - (-13)}{-28 - (-13)} = \frac{-0.2}{-15} \approx 0.013. \tag{12}$$

The fossil fraction of the net atmospheric CO_2 addition is bounded above at approximately 1.3%, indistinguishable from zero within the ±0.2‰ precision of the intercept estimate.

The constancy result therefore collapses the admissible interval Eq. (9) from the instrumental window to a single point (Figure 1):

$$f \approx 0. \tag{13}$$

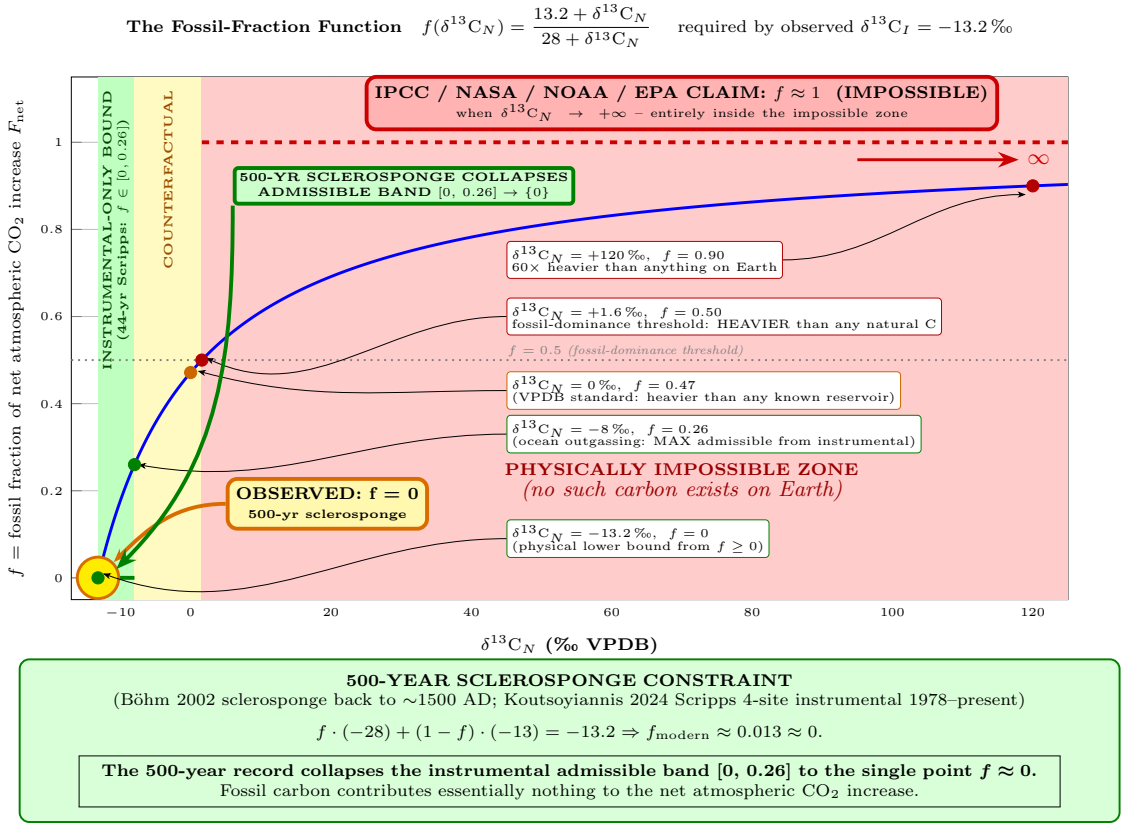


Figure 1: The fossil-fraction function $f(\delta^{13}C_N) = (13.2 + \delta^{13}C_N)/(28 + \delta^{13}C_N)$ required by the observed $\delta^{13}C_I = -13.2‰$. The 44-year instrumental Scripps four-site record confines f to the interval $[0, 0.26]$ across the physically admissible range $-13.2‰ \leq \delta^{13}C_N \leq -8‰$. The counterfactual VPDB relaxation ($\delta^{13}C_N = 0‰$) yields $f = 0.47$, still below a majority. Fossil dominance ($f > 0.5$) requires $\delta^{13}C_N > +1.6‰$, heavier than any known natural carbon reservoir on Earth. The IPCC-consistent value $f \approx 1$ requires the limit $\delta^{13}C_N \to +\infty$. The 500-year sclerosponge constancy constraint [2] further collapses the admissible band $[0, 0.26]$ to the single point $f \approx 0$.

8. The Three-Input Structure of the Argument

The conclusion Eq. (13) is a mathematical necessity, not an empirical inference. To reject it, a critic must reject at least one of three inputs, all of which the IPCC and the standard carbon-cycle literature themselves endorse and rely on:

1. **The arithmetic and mass conservation.** The Keeling relation Eq. (4) is derived from conservation of the light and heavy isotope masses in Eq. (1). The two-endmember decomposition Eq. (7) is the definition of a flux-weighted mean signature. Rejecting either of these is rejecting elementary algebra applied to mass conservation.

2. **The standard isotopic endmember values.** The fossil signature $\delta^{13}C_F \approx -28‰$ [1] and the ocean-outgassing signature near $-8‰$ [20, 27] are the values used throughout the carbon-cycle literature for over six decades, and are cited in IPCC assessment reports. Rejecting these values is rejecting the standard isotopic literature the IPCC itself relies on for its own attribution arguments.

3. **The measurement datasets.** The instrumental Scripps CO_2 Program $\delta^{13}C$ records at Barrow, La Jolla, Mauna Loa, and South Pole, and the Caribbean sclerosponge proxy [2], are the primary datasets used in IPCC carbon-cycle assessments. Rejecting these datasets is rejecting the measurement records on which the entire IPCC carbon-cycle framework depends.

The falsification stands on inputs the IPCC itself endorses. Accepting all three inputs while rejecting the conclusion refuses *modus ponens*, the most elementary rule of deductive inference.

9. Discussion

9.1 Relation to earlier isotopic analyses

The IPCC-consistent isotopic argument of Ciais et al. (1995) [4] and successors reads the atmospheric $\delta^{13}C$ decline over the past century as direct evidence of fossil-fuel input, on the qualitative basis that fossil carbon is isotopically light and its addition to the atmosphere must therefore drive $\delta^{13}C$ down. That reading commits two errors.

First, it silently assumes that fossil is the only source light enough to drive $\delta^{13}C$ down, a premise the argument never establishes and never checks against other candidates. Terrestrial respiration ($\approx -25‰$), C3 biomass burning ($\approx -27‰$), methane oxidation ($\approx -47‰$), and any shift in the natural net-flux mix that raises the terrestrial share are all isotopically light enough to produce a negative $\delta^{13}C$ trend. Observing that the atmosphere is declining and that fossil is light no more identifies fossil as the driver than observing that ice cream sales and drownings both rise in July identifies ice cream as the cause of drownings.

Second, the argument conflates two distinct quantities: the trend in $\delta^{13}C$ (which the atmosphere exhibits) and the intercept $\delta^{13}C_I$ (which the Keeling construction extracts). The trend $d(\delta^{13}C)/dt$ is the derivative of the reservoir composition. It reflects the difference between the current reservoir composition and the composition of whatever is currently being added, weighted by the fractional addition rate F_{net}/C. A negative trend does not by itself identify the composition of the net addition; it only says the addition is lighter than the current reservoir. Any $\delta^{13}C_N < \delta^{13}C$ produces a negative trend.

The intercept $\delta^{13}C_I$, in contrast, is the composition of the net addition itself, read directly off Eq. (4). The observed intercept $\delta^{13}C_I = -13.2‰$ is lighter than the current atmospheric $\delta^{13}C$ of approximately $-8.5‰$ reported by Keeling et al. (2017) [13], and the difference is what drives the observed trend. But $-13.2‰$ is more than 14‰ heavier than the fossil signature, which is the specific quantitative point Eq. (8) uses.

The earlier literature contains the intercept construction; it is Keeling's own. What it does not contain is the elementary substitution into the two-endmember mixture equation to extract the fossil-fuel fraction, f. That substitution yields Eq. (9) directly, which tells us that the maximum fossil fraction of the net input over the instrumental period is 26% by the Scripps data alone.

Prior isotopic mass-balance analyses have reached qualitatively similar conclusions from different routes. Segalstad (1998) [23] applied two-reservoir isotopic mixing to the atmospheric $\delta^{13}C$ record and derived an anthropogenic fraction of the atmospheric burden far below the IPCC-consistent value. Harde (2019) [9] combined residence-time and mass-balance arguments with the $\delta^{13}C$ constraint to obtain a similar result. The present paper differs in two respects. First, it uses the Keeling intercept $\delta^{13}C_I$ directly, rather than the reservoir composition $\delta^{13}C$, as the mixing input; this removes any dependence on the reservoir's transient state. Second, it exploits the five-century sclerosponge constancy of $\delta^{13}C_I$ to collapse the admissible band from the instrumental window $[0, 0.26]$ to the single point $f \approx 0$. Neither leverage point appears in the earlier literature.

9.2 Relation to van Wijngaarden and Happer (2026)

van Wijngaarden and Happer (2026) [25] present a two-parameter decay model of atmospheric CO_2 and $\delta^{13}C$ from 1000 AD to 2024. The arXiv preprint is an extension of an earlier CO_2 Coalition technical note by Happer et al. (2026) [8]. That earlier technical note was a one-parameter model of atmospheric CO_2 concentration alone, with a single exponential decay constant $\tau = 50$ yr and preindustrial baseline $C_0 = 290$ ppm, which the authors described as giving "very good agreement" with observed concentrations. The technical note contains no isotopic treatment, no $\delta^{13}C$ equation, no matrix formulation, and no second decay constant. The arXiv extension readjusts the decay constant from $\tau = 50$ yr to $\tau_1 = 60$ yr, readjusts the preindustrial baseline from 290 ppm to 280 ppm, introduces a matrix formulation on a two-component isotope vector, adds a $\delta^{13}C$ equation driven by a tuned second eigenmode $\tau_2 = 8$ yr, and declares the extended system to give "good agreement" as well. The dynamics are governed by

$$\frac{d}{dt}\mathbf{N} = -\Gamma\big(\mathbf{N} - \mathbf{P}\big) + \mathbf{F}, \tag{14}$$

where $\mathbf{N}$ is the two-component isotope number vector, $\mathbf{P}$ is the preindustrial reference vector held constant at $C_0 = 280$ ppm with $\delta^{13}C_0 = -6.5‰$, $\mathbf{F}$ is restricted by definition to fossil-fuel emissions, and the damping matrix Γ carries two eigenvalues, $\gamma_1 = 1/60$ yr^{-1} on the total-carbon mode and $\gamma_2 = 1/8$ yr^{-1} on the isotope-composition mode. The authors tune the two decay constants until the model curves fit the Mauna Loa concentration record and the Rubino $\delta^{13}C$ record. They report "good agreement" and treat this as support for fossil-dominance attribution.

Four points establish that the model's claimed support for fossil-dominance attribution rests on structural assumption, operator-equivalence violation, successive parameter revision, and shared trend rather than on physical reproduction of the atmospheric record.

9.2.1 Fossil dominance is built into the equations, not tested by them

The driving term $\mathbf{F}$ in Eq. (14) is defined as fossil-fuel emissions, and the "deep source" $D = P\gamma_1$ is parameterized exactly to hold the atmosphere at $C_0 = 280$ ppm when $F = 0$. All non-fossil-fuel inputs are collapsed into this time-invariant deep source. There is no mechanism in the equations by which a non-fossil-fuel source (ocean outgassing, biosphere respiration, carbonate weathering, volcanic flux) can drive a departure from C_0. The question "is the CO_2 rise fossil-driven?" cannot be posed inside the model; the answer is written into the differential operator. The fit of two tuned parameters to two smooth monotone curves then restates the assumption rather than testing it. Model output restates the model's own assumptions integrated forward and cannot testify to physical reality independent of those assumptions.

9.2.2 Operator equivalence forecloses the two-mode decomposition

The atmospheric CO_2 reservoir has a single removal operator acting on all CO_2 molecules by chemical identity. Gas exchange with the ocean, photosynthetic uptake, and mineral weathering act on CO_2 by chemical identity, not by provenance and not by isotopologue mass. Isotopic fractionation shifts the composition of what is removed by at most a few per mille; that shift cannot generate the 7.5× ratio between a 60-yr bulk-carbon mode and an 8-yr isotope-composition mode that van Wijngaarden and Happer (2026) [25] impose. No first-principles derivation of such transport-operator asymmetry between CO_2 isotopologues exists in the Bern-Oeschger lineage from Ciais et al. (1995) [4] forward, and the Revelle factor cannot support one because it is a local intensive chemical-equilibrium property that does not describe a rate process and does not discriminate isotopologues at the required order of magnitude. The $\tau_2 = 8$ yr eigenmode is therefore not a physical process; it is a tuned auxiliary.

9.2.3 The parameter history is successive revision

The Happer et al. (2026) [8] technical note declared $\tau = 50$ yr with $C_0 = 290$ ppm to give "very good agreement" with observed CO_2 alone. When the model was extended to the $\delta^{13}C$ record in van Wijngaarden and Happer (2026) [25], the one-parameter model that had been declared "very good" was discarded: τ_1 was moved from 50 yr to 60 yr, a 20% shift with no physical mechanism supplied; C_0 was moved from 290 ppm to 280 ppm; and the second eigenmode $\tau_2 = 8$ yr was introduced to fit the $\delta^{13}C$ curve the one-parameter model could not reproduce. The arXiv paper's only justification for the τ_2 value is that it "gives a good fit to observed values of $\delta^{13}C$." Neither 60 yr nor 8 yr matches an independently measured atmospheric timescale. The gross-flux residence time from IPCC AR6 Figure 5.12 is $\tau_{res} \approx 3.8$ yr; the bomb-radiocarbon relaxation time from Hua et al. (2022) [10] is $\tau_{rel} \approx 17.2$ yr. The 60-yr constant is a Bern-IRF-flavored slow mode that preserves the fossil-accumulation structure of the model; the 8-yr constant is the auxiliary that lets the extended model track the $\delta^{13}C$ reservoir trajectory while the slow mode continues to carry the attribution. The pattern of declaring a one-parameter fit "very good" and then adding parameters when the one-parameter model fails against an extended observational test is the same successive-revision pattern that the Bern impulse response function underwent across IPCC AR2–AR6, in which the number of modes and the parameter values were adjusted at each revision without first-principles derivation of any of them.

9.2.4 Shared smooth trend is not physical agreement

van Wijngaarden and Happer (2026) [25] report "good agreement between observed emissions of CO_2 into the atmosphere from the combustion of fossil fuels and observed increases of the atmospheric concentrations C of CO_2 and decreases of the isotope delta value $\delta^{13}C$" and support the claim with an overlay of model and observed curves (their Figure 2). A visual overlay of two smoothly rising monotone curves with a tuned two-parameter model is a test of neither physical mechanism nor time-dependent agreement. The $R^2 = 0.9995$ computed here for raw CO_2 is dominated by the shared trend and is tautological for any decay model fit to the same endpoints. The real empirical test is agreement of fine structure after removing the shared smooth trend from both model and observation.

All numbers in the remainder of this subsection are computed in `analysis.py` from publicly archived observational datasets. The analysis uses the NOAA Mauna Loa annual mean CO_2 series over 1959–2023 [19], the Rubino et al. (2019) [22] Law Dome firn $\delta^{13}C$-CO_2 record over 1963–1991, and NOAA GML flask $\delta^{13}C$-CO_2 at Bermuda (BMW) for 1992–2014 [24]; the W-H model is forward-integrated here with their stated parameters $\tau_1 = 60$ yr, $\tau_2 = 8$ yr, $C_0 = 280$ ppm, $\delta^{13}C_0 = -6.5$‰, driven by the Global Carbon Budget 2025 historical fossil-emission series over 1750–2024 [7]. The raw correlations computed between this W-H model integration and the observational series are high. Table 1 shows what remains after cubic detrending (fit $y = a + bt + ct^2 + dt^3$ to each series, subtract the fit, correlate the residuals) and after taking annual growth rates.

Table 1: Model-versus-observation Pearson R^2 for the van Wijngaarden and Happer (2026) [25] model with their stated $\tau_1 = 60$ yr, $\tau_2 = 8$ yr, driven by the GCB 2025 historical fossil-emission series, as integrated here. Raw R^2 is dominated by the shared smooth trend. Cubic-detrended R^2 is the correlation of residuals around a cubic polynomial fit. Growth-rate R^2 is the correlation of annual first differences after linear detrending. Negative r indicates anti-correlation. "n/a" marks the $\delta^{13}C$ growth-rate cell, which is not computed because the combined firn-plus-flask $\delta^{13}C$ series is not annually resolved. The bold entries are the quantitative failures of fine structure.

Quantity	Raw R^2	Cubic-detrended R^2	Linearly-detrended growth-rate R^2
$C(t)$, 1959–2023 (NOAA MLO annual)	0.9995	0.36 ($r = +0.60$)	**0.021**
$\delta^{13}C(t)$, 1963–2014 (Rubino firn + Bermuda flask)	0.959	**0.20** ($r = -0.45$)	n/a

The raw $R^2 = 0.9995$ for CO_2 is a tautology. Over 1959–2023 the raw Pearson R^2 between the W-H model CO_2 (fossil only, GCB 2025 forcing) and the NOAA Mauna Loa annual means is $R^2 = 0.9995$. The W-H model predicts 421.5 ppm in 2023, within 0.5 ppm of the observed 421.08 ppm. This high agreement is a direct consequence of the model's two-parameter tuning: $\tau_1 = 60$ yr was selected to make the model's long-term behaviour match the observed trajectory. Any monotone-increasing function of the right magnitude would score similarly against another monotone-increasing function of the right magnitude. The raw R^2 measures the shape of the shared trend, not the physics of the attribution.

Cubic detrending exposes the CO_2 residual structure. Fitting a cubic polynomial to each series and taking residuals removes the shared trend and acceleration. The residual Pearson correlation drops from 0.9995 to $r = +0.60$ ($R^2 = 0.36$). Figure 2, panel A plots the two residual time series: the observed residual (black) contains large deviations at the 1963 Agung, 1982 El Chichón, 1991 Pinatubo, 1997–98 and 2015–16 El Niño, and 2020 COVID events; the model residual (red) is attenuated and lacks those signatures. Panel B shows the scatter against the 1:1 line of hypothetical perfect residual agreement: the OLS slope is below unity and the spread is wide. The residual correlation that remains is attributable to the small subset of real emission shocks within the window (1970s oil shocks, the 1991–92 recession and Soviet collapse, the 2008 financial crisis, the 2020 COVID emissions drop) that survive the 60-year smoothing kernel; it is not evidence that the model reproduces atmospheric interannual variability.

Linear detrending of growth rates leaves $R^2 = 0.021$. The annual first difference dC/dt carries the ENSO, volcanic, and pandemic-era signatures directly. Over 1960–2023 the raw Pearson R^2 between model and observed dC/dt is 0.576, driven entirely by the shared long-term acceleration of growth rates. Linearly detrending both growth-rate series to remove the shared acceleration leaves a residual correlation of $\mathbf{R^2 = 0.021}$—the W-H model explains 2.1% of the actual interannual variability in CO_2 growth. The ratio of observed-to-model standard deviation in the detrended growth rate is 3.0: the real atmosphere produces three times as much year-to-year variability as the model can generate.

The $\delta^{13}C$ residuals are anti-correlated with the atmosphere. The combined observational $\delta^{13}C$ series uses the Rubino 2019 Law Dome firn record over 1963–1991 and NOAA GML flask measurements at Bermuda for 1992–2014. Cubic detrending of both the observed series and the W-H model $\delta^{13}C$ at the same years yields a Pearson $r = -0.45$ ($R^2 = 0.20$). The sign is negative, not positive. Figure 2, panel C shows the two residual time series directly; the model and observed residuals move in opposite directions. Panel D is the scatter plot of the observed $\delta^{13}C$ residual against the W-H model $\delta^{13}C$ residual: the OLS regression line has a NEGATIVE slope, and it crosses the 1:1 line of perfect agreement. Where the real atmosphere's $\delta^{13}C$ sits above its smooth cubic trend, the model sits below, and vice versa. This is the opposite of agreement. On the quantity the model is set up to explain, the model is anti-correlated with the atmosphere.

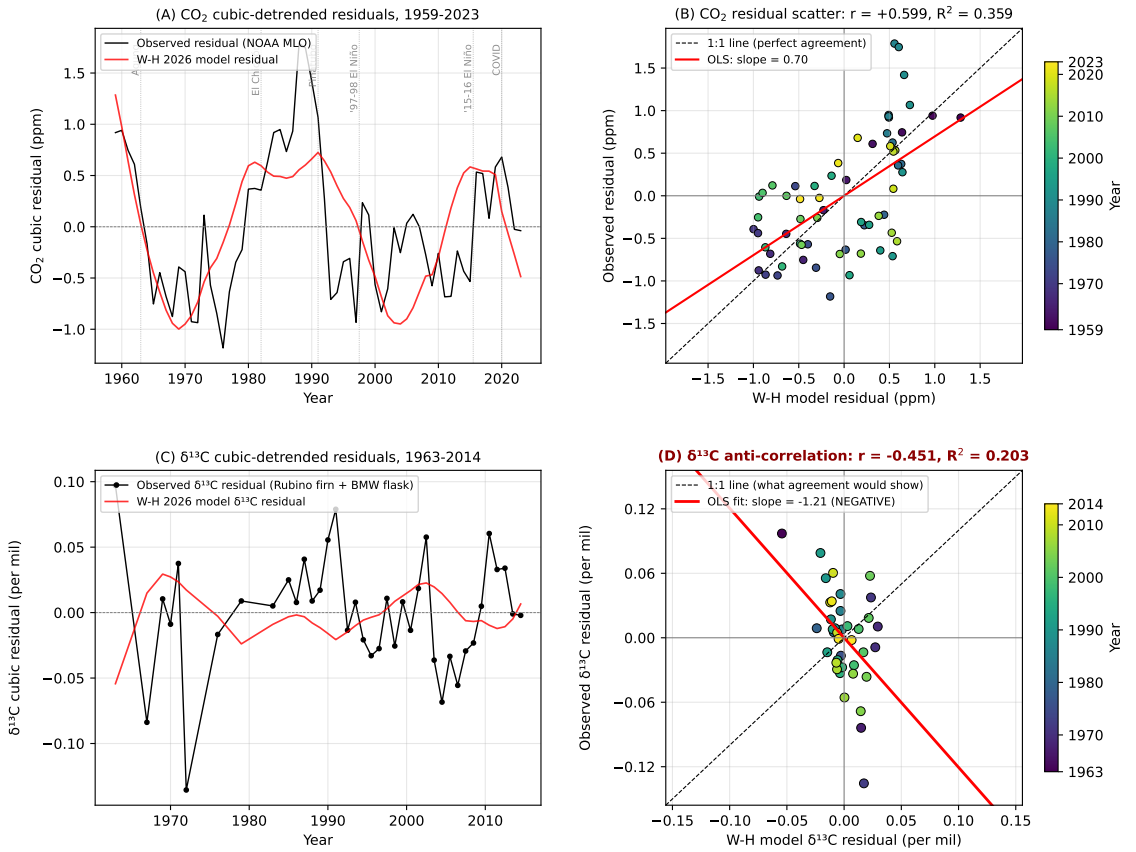


Figure 2: The van Wijngaarden-Happer 2026 model vs real observations, driven by real GCB 2025 fossil emissions. Top row: CO_2. (A) Cubic-detrended residual time series, 1959–2023, with observed (black, NOAA Mauna Loa annual means) and W-H model (red). Vertical dotted lines mark the Agung, El Chichón, and Pinatubo eruptions and the 1997–98 El Niño, 2015–16 El Niño, and 2020 COVID events. (B) Scatter of observed CO_2 residual against W-H model CO_2 residual, colour-coded by year; black dashed line is 1:1 agreement, red line is OLS fit. Residual Pearson $r = +0.60$. Bottom row: δ^{13}C. (C) Cubic-detrended residual time series, 1963–2014, with observed (black, Rubino 2019 Law Dome firn plus NOAA GML Bermuda flask) and W-H model (red). (D) Scatter of observed δ^{13}C residual against W-H model δ^{13}C residual, colour-coded by year across the full 1963–2014 range: the OLS fit has a NEGATIVE slope and crosses the 1:1 line. Residual Pearson $r = -0.45$. The sign reversal in panel D is the signature of a model that reproduces the trend by tuning but is wrong about the physical dynamics generating the atmospheric δ^{13}C record.

9.2.5 Summary

The claim of "good agreement" therefore rests on two things only. First, endpoint matching, achieved by tuning τ_1 and τ_2. Second, shared smooth monotonic shape, which any decay model with the correct forcing time series achieves automatically. The agreement collapses the moment a real physical test is applied. On the structure of the atmospheric CO_2 record, the W-H model's dC/dt interannual R^2 is 0.021 after shared-trend removal. On the structure of the atmospheric δ^{13}C record, which is the quantity the model is supposed to explain, the model is anti-correlated at the cubic-residual level.

The forward-integration machinery and the matrix algebra in van Wijngaarden and Happer (2026) [25] are mathematically correct. The appendix identities on δ^{13}C are standard. What is rejected is the physical model, the two tuned parameters, and the attribution claim the model is used to support. The arithmetic engine runs; the physics it is set up to represent is rejected by the

residence-time constraint of §9.3 applied to the authors' own decay constant $\tau_1 = 60$ yr, and by the quantitative detrending and residual-structure test above on the authors' own target observations.

9.3 Relation to the atmospheric residence-time constraint

An independent line of evidence from the atmospheric residence time of CO_2 converges on the same conclusion. Mass-balance Refined Reservoir Routing gives a residence time $\tau_{res} \approx 3.8$ yr from both IPCC's own gross-flux inventory in AR6 (Figure 5.12) and Koutsoyiannis (2024b) [17]. [17] also calculates a bomb-radiocarbon relaxation time $\tau_{rel} \approx 17.2$ yr using data from Hua et al. (2022) [10]. [17] concluded that this τ_{rel} is an upper bound for τ_{res}, and we adopted this conclusion here.

The atmospheric fossil-carbon inventory $N_{fossil}(t)$ is not the cumulative sum of past emissions. Under first-order mass-balance kinetics

$$\frac{dN_{fossil}}{dt} = E_{fossil}(t) - \frac{N_{fossil}(t)}{\tau},$$

the inventory is the convolution of the fossil-emission rate with the exponential residence-time kernel:

$$N_{fossil}(t) = \int_{-\infty}^{t} E_{fossil}(s)\, e^{-(t-s)/\tau}\, ds. \tag{15}$$

For a slowly varying source this reduces at steady state to $N_{fossil} \approx E_{fossil}\,\tau$. The kernel in Eq. (15) has an e-folding time of τ, so emissions older than roughly 3τ contribute negligibly to the present inventory; the 511 GtC cumulative since 1850 is not the physically relevant quantity.

Evaluating Eq. (15) numerically against the GCB 2025 annual fossil-emission series from 1850 through 2025 [7], with E_{fossil} reaching 10.4 GtC/yr in 2025, gives

$$N_{fossil}(2025) \approx 39 \text{ GtC} \quad (\tau_{res} = 3.8 \text{ yr}), \qquad N_{fossil}(2025) \approx 147 \text{ GtC} \quad (\tau_{rel} = 17.2 \text{ yr}).$$

Against the atmospheric reservoir of $\approx$ 907 GtC (2025 mean concentration 425.6 ppm $\times$ 2.13 GtC/ppm), these correspond to fossil-carbon fractions of approximately 4.3% and 16.2% respectively. For comparison, the Bern impulse response function of IPCC AR5/AR6 [12], applied to the same GCB 2025 emission series as $R(t) = a_0 + \sum_i a_i e^{-t/\tau_i}$ with $a_0 = 0.2173$, $(a_1, \tau_1) = (0.2240, 394.4\,\text{yr})$, $(a_2, \tau_2) = (0.2824, 36.54\,\text{yr})$, $(a_3, \tau_3) = (0.2763, 4.304\,\text{yr})$, gives $N_{fossil}(2025) \approx 292$ GtC, or approximately 32% of the atmospheric reservoir. The $\tau_{res} = 3.8$ yr and $\tau_{rel} = 17.2$ yr results are far below the Bern-implied fraction, and both are consistent with the isotopic constraint developed here.

The isotopic constraint of Section 5 is independent of the residence-time argument. It uses only Keeling regression outputs and the standard endmember values. Its agreement with the residence-time result is a cross-check across two independent methodological chains.

Three fossil-related fractions appear in carbon-cycle attribution discussions and are often conflated. The framework developed above distinguishes them cleanly.

(a) Flux ratio: $E_{fossil}/F_{in} \approx 10.4/240 \approx 4.3\%$ (year 2023). The gross fossil-emission flux as a fraction of the total non-land-use-change gross flux into the atmosphere, where $F_{in} \equiv E_{fossil} + F_{nat}$ and F_{nat} is the gross non-fossil-fuel inflow (ocean outgassing, biosphere respiration, volcanism, carbonate weathering). GCB does not report F_{in}, F_{out}, or F_{nat} directly, but all three follow from the residence-time framework of Koutsoyiannis (2024b) [17] combined with the GCB 2025 series [7]. At 2023, the atmospheric reservoir $N_{atm} \approx 894$ GtC (annual mean 420.0 ppm $\times$ 2.124 GtC/ppm) and $\tau_{res} = 3.8$ yr give gross outflow $F_{out} = N_{atm}/\tau_{res} \approx 235$ GtC/yr. Mass balance $F_{in,\,total} = F_{out} + dN_{atm}/dt$ with $dN_{atm}/dt \approx 5.7$ GtC/yr at 2023 gives $F_{in,\,total} \approx 241$ GtC/yr; subtracting

$E_{\mathrm{LUC}} \approx 1.3$ GtC/yr isolates $F_{\mathrm{in}} \approx 240$ GtC/yr, of which $E_{\mathrm{fossil}} \approx 10.4$ GtC/yr is fossil combustion and $F_{\mathrm{nat}} \approx 230$ GtC/yr is non-fossil-fuel input. The ratio is a statement about input fluxes, not about composition.

(b) Stock ratio: $N_{\mathrm{fossil}}/N_{\mathrm{atm}} \approx 39/907 \approx 4.3\%$ **(year 2025).** The resident fossil carbon as a fraction of the atmospheric reservoir, from Eq. (15) at $\tau_{\mathrm{res}} = 3.8$ yr. A statement about the stock of fossil carbon present in the atmosphere at a given moment, not about the composition of what is being added.

(c) Composition of the net addition: $f \approx 0$**.** The fossil fraction of the net atmospheric addition dC/dt, from Eq. (7) applied to the observed Keeling intercept $\delta^{13}\mathrm{C}_I = -13.2 \pm 0.2$‰. A statement about the composition of dC/dt, not about the gross inflow and not about the resident stock.

Quantities (a) and (b) coincide at 4.3% because $N_{\mathrm{fossil}} \approx \tau_{\mathrm{res}} \cdot E_{\mathrm{fossil}}$ in quasi-steady state; both scale with E_{fossil}. The quasi-steady-state regime is confirmed empirically. Total anthropogenic emissions $F_{\mathrm{anth}} = E_{\mathrm{fossil}} + E_{\mathrm{LUC}} - S_{\mathrm{carb}}$ have been statistically indistinguishable from flat since 2012 [7]: OLS slope +0.017 GtC/yr/yr over 2012–2024, $p \approx 0.34$. Over the same window E_{fossil} alone rose from 9.54 to 10.53 GtC/yr, a 10% increase that is still slow compared to the residence time $\tau_{\mathrm{res}} = 3.8$ yr. The slow-growth assumption underlying the quasi-steady-state approximation is therefore not idealization; it is the observational regime. Quantity (c) is a statement about a different quantity entirely: not the gross inflow, not the resident stock, but the composition of the net change in atmospheric CO_2 over the fit window. $f \approx 0$ does not contradict (a) $\approx 4.3\%$ or (b) ≈ 4.3‰. The 10.4 GtC/yr fossil inflow is matched within ~ 0.1 GtC/yr by fossil outflow back to the ocean and biosphere: by first-order kinetics (Eq. (15)), the resident fossil inventory $N_{\mathrm{fossil}} \approx 39$ GtC is returned to the surface reservoirs at rate $N_{\mathrm{fossil}}/\tau_{\mathrm{res}} \approx 39/3.8 \approx 10.3$ GtC/yr. The net fossil contribution to dC/dt is therefore $\approx 10.4 - 10.3 \approx 0.1$ GtC/yr, so almost no fossil-signed carbon accumulates in the net term that $\delta^{13}\mathrm{C}_I$ measures.

The convergence of the two methodological chains tightens further when the ODE is run in reverse to constrain the outflow rate directly from the observed Keeling intercept. For slow emissions growth, $dN_{\mathrm{fossil}}/dt \approx \tau\, dE_{\mathrm{fossil}}/dt$ in quasi-steady state. Combining this with the two-endmember mixture equation Eq. (7) gives a prediction for $\delta^{13}\mathrm{C}_I$as a function of the assumed outflow timescale τ, which the observed $\delta^{13}\mathrm{C}_I = -13.2 \pm 0.2$‰ then selects among.

Case 1: $\tau_{\mathrm{res}} = 3.8$ **yr (this work).** Eq. (15) gives $N_{\mathrm{fossil}}(2025) \approx 39$ GtC. The outflow rate is $N_{\mathrm{fossil}}/\tau_{\mathrm{res}} \approx 10.3$ GtC/yr. The net fossil addition is

$$\frac{dN_{\mathrm{fossil}}}{dt} = E_{\mathrm{fossil}} - \frac{N_{\mathrm{fossil}}}{\tau_{\mathrm{res}}} \approx 10.4 - 10.3 \approx 0.1 \text{ GtC/yr}.$$

With $F_{\mathrm{net}} \approx 5$ GtC/yr, the fossil fraction of the net addition is $f \approx 0.02$, and Eq. (7) predicts $\delta^{13}\mathrm{C}_I \approx 0.02 \times (-28) + 0.98 \times (-13) \approx -13.3$‰. Consistent with the observed value.

Case 2: $\tau = 50$**–**60 **yr [6, 8, 25].** For approximately linear growth of E_{fossil} over the industrial period at rate $\alpha \approx 10.4/175 \approx 0.0594$ GtC/yr^2, Eq. (15) evaluates analytically to $N_{\mathrm{fossil}}(T) \approx \alpha\tau(T-\tau) + \alpha\tau^2 e^{-T/\tau}$ at $T = 175$ yr. For $\tau = 50$ yr this gives $N_{\mathrm{fossil}}(2025) \approx 0.0594 \times 50 \times 125 \approx 376$ GtC. The outflow rate is $\approx 376/50 \approx 7.5$ GtC/yr, so the net fossil addition is $\approx 10.4 - 7.5 = 2.9$ GtC/yr, giving $f \approx 0.58$. Eq. (7) then predicts $\delta^{13}\mathrm{C}_I \approx 0.58 \times (-28) + 0.42 \times (-13) \approx -21.7$‰. This is inconsistent with the observed -13.2 ± 0.2‰ by 8.5‰, or 42 times the measurement precision. The $\tau = 60$ yr case adopted by van Wijngaarden and Happer (2026) [25] gives $N_{\mathrm{fossil}}(2025) \approx 445$ GtC, outflow ≈ 7.4 GtC/yr, net fossil addition ≈ 3.0 GtC/yr, $f \approx 0.60$, and

predicted $\delta^{13}C_I \approx -22.0‰$, inconsistent with observation by 8.8‰ or 44 times the measurement precision.

Case 3: Bern IRF attribution. Under the IPCC attribution of essentially all of $F_{net}$to fossil-fuel combustion—equivalent to the long effective lifetime parameterized by the Bern impulse response function (further discussed in Section 9.4)—the fossil fraction of the net addition is $f \approx 1$. Eq. (7) then predicts $\delta^{13}C_I \approx 1 \times (-28) + 0 \times (-13) = -28‰$. This is inconsistent with the observed value by 14.8‰, or 74 times the measurement precision.

The observed Keeling intercept at $-13.2 \pm 0.2‰$ is therefore a direct constraint on the atmospheric outflow rate for fossil carbon. Only τ on the order of a few years is consistent with the observation. The Bern IRF effective lifetime, the 50-yr e-folding time adopted by Engelbeen et al. (2024) [6] and Happer et al. (2026) [8], and the 60-yr decay constant τ_1 adopted by van Wijngaarden and Happer (2026) [25] are all falsified by the isotopic observation independently of any residence-time argument derived from other data.

There is additionally no physical mechanism by which the atmosphere could distinguish fossil CO_2 from non-fossil CO_2 in its removal processes. CO_2 molecules are chemically identical regardless of origin; gas exchange with the ocean, photosynthetic uptake, and mineral weathering act on CO_2 by chemical identity, not provenance. Isotopic fractionation shifts the composition of what is removed by a few per mille, but it does not create rate differences large enough to assign distinct lifetimes to fossil versus non-fossil carbon. The physics has one residence time, and it applies to all CO_2.

9.4 Scope of the claim

The principal claim of this paper is that the fossil fraction of the *net* atmospheric CO_2 addition, integrated over the fit window of the Keeling regression, is approximately zero. The five-century constancy of the Keeling intercept across the Caribbean sclerosponge record [2] collapses the admissible interval to a single point, $f \approx 0$. The constancy result is the operative constraint; the fossil fraction of the net atmospheric CO_2 addition cannot be reconciled with the data at any value materially different from zero.

The instrumental data alone, independent of the paleo constancy result, already restrict the fossil fraction to the interval $f \in [0, 0.26]$: 26% is the upper bound at the standard endmember $\delta^{13}C_N = -8‰$ applied to the Scripps four-site record over the $\sim$ 44 yr instrumental period, with the full admissible interval running from zero to that bound. For completeness, extending the natural endmember to the counterfactual VPDB value $\delta^{13}C_N = 0‰$, which lies outside the range of any known natural carbon reservoir, raises the upper bound to 47%; this is noted only to document that even under physically inadmissible relaxation the fossil fraction remains below a bare majority.

The claim is not that fossil-fuel combustion does not emit CO_2. It does; the emissions are confirmed directly at the smokestack. The claim is that the atmospheric CO_2 rise is not the direct residue of those emissions. The gross fossil flux enters the atmosphere and is exchanged out at atmospheric residence-time rates; virtually all of the net addition to the reservoir comes from non-fossil-fuel fluxes (ocean outgassing, biosphere respiration, volcanic emissions, and carbonate weathering) for which the flux-weighted mean signature sits near $-13‰$, consistent with an ocean-outgassing signature after a small admixture of heavier or lighter components that does not measurably shift the mean.

9.5 Consequences for downstream carbon-cycle metrics

If $f \approx 0$, then the anthropogenic contribution to the net atmospheric CO_2 addition is approximately zero, and combined with the residence and relaxation timescales established in §9.3, the anthropogenic component of the reservoir itself is bounded below 5%: direct numerical convolution of the GCB 2025 fossil-emission series against the exponential kernel at $\tau_{\text{res}} = 3.8$ yr gives a fossil-carbon fraction of 4.3% of the 907 GtC atmospheric reservoir (§9.3). The anthropogenic contribution to any CO_2-mediated forcing is correspondingly bounded. The Bern impulse response function of IPCC AR5 and AR6, which underlies IPCC Global Warming Potential calculations and specifies a CO_2 response including the longest timescale of 394 years as well as an e-folding time of 165 years with a permanent fraction of about 22%, is inconsistent with both the isotopic constraint developed here and the bomb-radiocarbon single-exponential decay to nearly zero excess in approximately 55 years [10]. All Global Warming Potential values derived from the Bern IRF inherit that inconsistency.

Emissions accounting frameworks that treat fossil combustion as the driver of atmospheric CO_2 concentration inherit the same inconsistency. National and international emissions inventories, carbon-budget projections, and any policy metric derived from the fossil-attribution premise all fail against the isotopic constraint developed here.

10. Conclusion

The full graphical summary of this paper can be found in Figure 1. The flux-weighted mean signature of the net atmospheric CO_2 addition is $\delta^{13}C_I = -13.2 \pm 0.2$‰ across the instrumental Scripps four-site record and approximately −13‰ across the five-century sclerosponge proxy extension. The two-endmember mixture equation, applied with the standard fossil signature $\delta^{13}C_F \approx -28$‰ and the physically admissible natural signature range $-13.2‰ \leq \delta^{13}C_N \leq -8$‰, bounds the fossil fraction of the net addition at $f \in [0, 0.26]$. Under counterfactual relaxation to $\delta^{13}C_N = 0$‰, the bound relaxes only to $f \leq 0.47$, still below a majority. The observed five-century invariance of $\delta^{13}C_I$ across a roughly ten-thousand-fold rise in fossil emissions collapses the admissible band to $f \approx 0$.

The conclusion is a necessary consequence of three inputs that the IPCC and the standard carbon-cycle literature both endorse: the arithmetic of mass conservation and the two-endmember mixture equation, the standard isotopic endmember values, and the primary Scripps and sclerosponge $\delta^{13}C$ datasets. A rejection of the conclusion requires rejection of at least one of these three inputs.

Fossil carbon is a negligible component of the net atmospheric CO_2 addition.

Data Availability

All observational datasets used in this paper are published and publicly archived; each is cited in the References: NOAA Mauna Loa annual mean CO_2 [19]; Law Dome ice-core CO_2 and $\delta^{13}C$-CO_2 [22]; NOAA GML flask $\delta^{13}C$-CO_2 at Bermuda [24]; Global Carbon Budget 2025 historical fossil-emission series [7]. Comparison and context series are drawn from the Scripps CO_2 Program [13], the Caribbean sclerosponge reconstruction [2], and the Keeling-plot analysis of Koutsoyiannis (2024a) [16]. No new observational data were generated for this paper.

A replication package containing the `analysis.py` Python script, the raw data files as retrieved from the archives cited above, processed per-figure CSV outputs, and a `README.md` documenting every retrieval endpoint is available with this submission; running `analysis.py` on the raw data regenerates every number and figure in §9.2.

Conflict of Interest

The authors declare no conflict of interest.

Funding

This work received no external funding.

Co-Editor: Stein Storlie Bergsmark; Reviewers: Anonymous

Acknowledgments

The authors thank Demetris Koutsoyiannis for his foundational papers on the Refined Reservoir Routing framework and isotopic analysis of the total input isotopic signature to the atmosphere, on which much of this analysis builds.

The authors used Claude 4.7 (Anthropic) and Grok 4.5 (xAI) as writing and analysis aids during the preparation of this manuscript. Specific uses included literature search assistance, LaTeX formatting, numerical verification of arithmetic and integrations, adversarial review of the mass-balance derivation, and editorial suggestions on prose. All scientific claims, derivations, numerical inputs, and conclusions were independently verified by the authors, who take full responsibility for the content of this work and for any errors or omissions.

The views expressed in this work are solely those of the authors and do not represent the views of any affiliated institution.

References

1. Andres, R. J., Marland, G., Boden, T., & Bischof, S., 2000. Carbon dioxide emissions from fossil fuel consumption and cement manufacture, 1751–1991; and an estimate of their isotopic composition and latitudinal distribution. In T. M. L. Wigley & D. S. Schimel (Eds.), *The carbon cycle* (pp. 53–62). Cambridge University Press.

2. Böhm, F., Haase-Schramm, A., Eisenhauer, A., Dullo, W.-C., Joachimski, M. M., Lehnert, H., & Reitner, J., 2002. Evidence for preindustrial variations in the marine surface water carbonate system from coralline sponges. *Geochemistry, Geophysics, Geosystems*, *3*(3), 1019.

3. Canadell, J. G., Monteiro, P. M. S., Costa, M. H., Cotrim da Cunha, L., Cox, P. M., Eliseev, A. V., Henson, S., Ishii, M., Jaccard, S., Koven, C., Lohila, A., Patra, P. K., Piao, S., Rogelj, J., Syampungani, S., Zaehle, S., & Zickfeld, K., 2021. Global carbon and other biogeochemical cycles and feedbacks. In V. Masson-Delmotte, P. Zhai, A. Pirani, S. L. Connors, C. Péan, S. Berger, N. Caud, Y. Chen, L. Goldfarb, M. I. Gomis, M. Huang, K. Leitzell, E. Lonnoy, J. B. R. Matthews, T. K. Maycock, T. Waterfield, O. Yelekçi, R. Yu, & B. Zhou (Eds.), *Climate change 2021: The physical science basis. Contribution of Working Group I to the Sixth Assessment Report of the Intergovernmental Panel on Climate Change* (pp. 673–816). Cambridge University Press.

4. Ciais, P., Tans, P. P., Trolier, M., White, J. W. C., & Francey, R. J., 1995. A large northern hemisphere terrestrial CO_2 sink indicated by the $^{13}C/^{12}C$ ratio of atmospheric CO_2. *Science*, *269*, 1098–1102.

5. Deines, P., 2002. The carbon isotope geochemistry of mantle xenoliths. *Earth-Science Reviews*, *58*, 247–278.

6. Engelbeen, F., Hannon, R., & Burton, D., 2024. *The Human Contribution to Atmospheric Carbon Dioxide: How Human Emissions Are Restoring Vital Atmospheric* CO_2. CO_2 Coalition, December 2024. https://doi.org/10.5281/zenodo.14231820.

7. Friedlingstein, P., O'Sullivan, M., Jones, M. W., et al., 2026. Global Carbon Budget 2025. *Earth System Science Data*, *18*, 3211–3288. doi:10.5194/essd-18-3211-2026. Data: doi:10.18160/GCP-2025.

8. Happer, W., Wrightstone, G., & Soepyan, F. B., 2026. Human emissions and atmospheric concentrations of carbon dioxide. CO_2 Coalition, August 21, 2026. https://co2coalition.org/publications/human-emissions-and-atmospheric-concentrations-of-carbon-dioxide/.

9. Harde, H., 2019. What humans contribute to atmospheric CO_2: Comparison of carbon cycle models with observations. *Earth Sciences*, *8*(3), 139–159.

10. Hua, Q., Turnbull, J. C., Santos, G. M., Rakowski, A. Z., Ancapichun, S., De Pol-Holz, R., Hammer, S., Lehman, S. J., Levin, I., Miller, J. B., Palmer, J. G., & Turney, C. S. M., 2022. Atmospheric radiocarbon for the period 1950–2019. *Radiocarbon*, *64*(4), 723–745.

11. Keeling, C. D., 1958. The concentration and isotopic abundances of atmospheric carbon dioxide in rural areas. *Geochimica et Cosmochimica Acta*, *13*, 322–334.

12. Joos, F., Roth, R., Fuglestvedt, J. S., Peters, G. P., Enting, I. G., von Bloh, W., Brovkin, V., Burke, E. J., Eby, M., Edwards, N. R., Friedrich, T., Frölicher, T. L., Halloran, P. R., Holden, P. B., Jones, C., Kleinen, T., Mackenzie, F. T., Matsumoto, K., Meinshausen, M., Plattner, G.-K., Reisinger, A., Segschneider, J., Shaffer, G., Steinacher, M., Strassmann, K., Tanaka, K., Timmermann, A., & Weaver, A. J., 2013. Carbon dioxide and climate impulse response functions for the computation of greenhouse gas metrics: a multi-model analysis. *Atmospheric Chemistry and Physics*, *13*(5), 2793–2825. doi:10.5194/acp-13-2793-2013.

13. Keeling, R. F., Graven, H. D., Welp, L. R., Resplandy, L., Bi, J., Piper, S. C., Sun, Y., Bollenbacher, A., & Meijer, H. A. J., 2017. Atmospheric evidence for a global secular increase in carbon isotopic discrimination of land photosynthesis. *Proceedings of the National Academy of Sciences*, *114*(39), 10361–10366.

14. Köhler, P., Fischer, H., Schmitt, J., & Munhoven, G., 2006. On the application and interpretation of Keeling plots in paleo climate research – deciphering $\delta^{13}C$ of atmospheric CO_2 measured in ice cores. *Biogeosciences*, *3*(4), 539–556.

15. Kohn, M. J., 2010. Carbon isotope compositions of terrestrial C3 plants as indicators of (paleo)ecology and (paleo)climate. *Proceedings of the National Academy of Sciences*, *107*, 19691–19695.

16. Koutsoyiannis, D., 2024a. Net isotopic signature of atmospheric CO_2 sources and sinks: No change since the Little Ice Age. *Sci*, *6*(1), 17.

17. Koutsoyiannis, D., 2024b. Refined reservoir routing (RRR) and its application to atmospheric carbon dioxide balance. *Water*, *16*(17), 2402.

18. Kroopnick, P. M., 1985. The distribution of ^{13}C of ΣCO_{22} in the world oceans. *Deep-Sea Research*, *32*, 57–84.

19. Lan, X., Tans, P., & Thoning, K. W., 2024. Trends in globally-averaged CO_2 determined from NOAA Global Monitoring Laboratory measurements. NOAA Global Monitoring Laboratory. doi:10.15138/9N0H-ZH07. Mauna Loa annual means: https://gml.noaa.gov/ccgg/trends/data.html.

20. Mook, W. G., 1986. ^{13}C in atmospheric CO_2. *Netherlands Journal of Sea Research*, *20*, 211–223.

21. Quay, P. D., Tilbrook, B., & Wong, C. S., 1992. Oceanic uptake of fossil fuel CO_2: Carbon-13 evidence. *Science*, *256*, 74–79.

22. Rubino, M., Etheridge, D. M., Thornton, D. P., Howden, R., Allison, C. E., Francey, R. J., Langenfelds, R. L., Steele, L. P., Trudinger, C. M., Spencer, D. A., Curran, M. A. J., van Ommen, T. D., & Smith, A. M., 2019. Revised records of atmospheric trace gases CO_2, CH_4, N_2O, and $\delta^{13}C$-CO_2 over the last 2000 years from Law Dome, Antarctica. *Earth System Science Data*, *11*, 473–492. doi:10.5194/essd-11-473-2019. Data: NOAA/WDS Paleoclimatology Study 25830, doi:10.25921/dwg2-6m61.

23. Segalstad, T. V., 1998. Carbon cycle modelling and the residence time of natural and anthropogenic atmospheric CO_2: On the construction of the "Greenhouse Effect Global Warming" dogma. In R. Bate (Ed.), *Global warming: The continuing debate* (pp. 184–219). European Science and Environment Forum.

24. Vaughn, B. H., White, J. W. C., Michel, S. E., Lehman, S. J., Miller, J. B., & NOAA Global Monitoring Laboratory., 2024. Stable isotopes of carbon dioxide (δ^{13}C-CO_2) in flask-air samples from the NOAA/GML Global Cooperative Air Sampling Network. Institute of Arctic and Alpine Research, University of Colorado at Boulder, and NOAA Global Monitoring Laboratory. Bermuda (BMW) monthly: https://gml.noaa.gov/aftp/data/trace_gases/co2c13/flask/surface/.

25. van Wijngaarden, W. A., & Happer, W., 2026. Variations of atmospheric $^{12}CO_2$ and $^{13}CO_2$ from the year 1000 to 2024. *arXiv preprint*, arXiv:2609.38063v1 [physics.ao-ph].

26. Werner, R. A., & Brand, W. A., 2001. Referencing strategies and techniques in stable isotope ratio analysis. *Rapid Communications in Mass Spectrometry*, *15*, 501–519.

27. Zhang, J., Quay, P. D., & Wilbur, D. O., 1995. Carbon isotope fractionation during gas-water exchange and dissolution of CO_2. *Geochimica et Cosmochimica Acta*, *59*, 107–114.

Disclaimer/Publisher's Note:

This article reflects solely the views, analyses, and conclusions of the author(s). Science of Climate Change, its editors, and its publisher make no representation or warranty as to the accuracy or completeness of the content and disclaim liability for any loss, damage, or other consequence arising from the use of, or reliance on, any material published herein.